

Ultraviolet to Near-infrared Single Photon Emitters in hBN

Qing-Hai Tan^{1,2}, Xue-Lu Liu^{1,2}, Dan Guo^{1,2}, Yong-Zhou Xue^{1,2}, Shu-Liang Ren^{1,2}, Yuan-Fei Gao¹,
Xiu-Ming Dou^{1,2}, Bao-Quan Sun^{1,2}, Hui-Xiong Deng^{1,2}, Ping-Heng Tan^{1,2}, and Jun Zhang^{1,2,3,4*}

¹State Key Laboratory of Superlattices and Microstructures,
Institute of Semiconductors, Chinese Academy of Sciences, Beijing 100083,

China ²Center of Materials Science and Optoelectronics Engineering,
University of Chinese Academy of Sciences, Beijing 100049,

China ³CAS Center of Excellence in Topological Quantum Computation,
University of Chinese Academy of Sciences, Beijing 101408,

China ⁴Beijing Academy of Quantum Information Science, Beijing 100193, China

*Correspondence and requests for materials should be addressed to J. Z. (Email: zhangjwill@semi.ac.cn)

In the field of quantum photon sources, single photon emitter from solid is of fundamental importance for quantum computing, quantum communication, and quantum metrology. However, it has been an ultimate but seemingly distant goal to find the single photon sources that stable at room or high temperature, with high-brightness and broad ranges emission wavelength that successively cover ultraviolet to infrared in one host material. Here, we report an ultraviolet to near-infrared broad-spectrum single photon emitters (SPEs) based on a wide band-gap semiconductor material hexagonal boron nitride (hBN). The bright, high purity and stable SPEs with broad-spectrum are observed by using the resonant excitation technique. The single photon sources here can be operated at liquid helium, room temperature and even up to 1100 K. Depending on the excitation laser wavelengths, the SPEs can be dramatically observed from 357 nm to 896 nm. The single photon purity is higher than to 90 percentage and the narrowest linewidth of SPE is down to $\sim 75 \mu\text{eV}$ at low temperature, which reaches the resolution limit of our spectrometer. Our work not only paves a way to engineer a monolithic semiconductor tunable SPS, but also provides fundamental experimental evidence to understand the electronic and crystallographic structure of SPE defect states in hBN.

Solid-state single photon sources (SPSs) play a fundamental role in quantum technologies including quantum computing, quantum secure communication, and quantum metrology¹⁻⁵. Over the past decade, many solid-state single photon emitters (SPEs) have been developed such as the originally studied color centers², quantum dots (QDs)^{6,7}, carbon nanotubes (CNTs)⁸, as well as recently emerged SPEs in two-dimensional (2D) materials⁹. The SPEs in monolayer WSe₂¹⁰⁻¹³, and WS₂^{14,15} have been observed at liquid Helium temperature from localized bound excitons. However, up to now, most of these reported SPSs are limited in a narrow spectral range at Liquid-helium cryogenic temperatures^{1,2}. Wide bandgap Gallium-Nitride QDs enables high-temperature operation of solid-state SPSs with emission wavelengths spanning from ultraviolet (UV) (286 nm)¹⁶, red (600-750 nm)¹⁷ and infrared (1100-1300 nm)¹⁸, but it is difficult to achieve a full spectral range of SPEs in one chip because the different doping and quantum structures are required to realize a specific emission wavelength. Since each range of SPS has its own unique application and urgent on-demand in quantum technologies. For example, the ultraviolet SPSs can be used for smaller size quantum-optical devices¹⁹, the near infrared SPSs at telecom wavelength range can be used to realize quantum key distribution and wireless communication¹⁸. Therefore, it is significant to achieve a bright and stable SPEs covering ultraviolet to the near-infrared spectrum and can work over a wide temperature range with just

one host material. In hexagonal boron nitride (hBN), the SPEs have been associated with deep energy level defect states within the large band gap that allow a bright and stable SPE at room temperature and even higher temperature²⁰⁻³⁷. Atom-like defects in hBN confine electronic levels deeply within the larger band gap, resulting in stable and extremely robust SPSs. Currently, the light-excited SPEs of hBN were found mostly distributed within 550 nm to 800 nm spectral ranges at room temperature^{24,38,39}. And an ultraviolet (UV) SPEs at 150 K was observed by cathodoluminescence spectroscopy combined with a scanning transmission electron microscope (STEM)²⁶. All of these results indicate that the hBN should be one of the promising host materials to achieve full spectral range from ultraviolet to near-infrared SPSs at room temperature and even higher temperature. To the best of our knowledge, such an hBN based SPS have not been reported.

Here, we report the realization of a light-pumped broadband SPEs covering from 357 to 896 nm in hBN flakes. The strict excitation selectivity is observed by photoluminescence excitation (PLE) spectroscopy, which reveals the multi-level nature of defect emitters in hBN and indicates that the resonant excitation is a good way to achieve the high bright and tunable SPS in hBN. In particular, these SPE peaks can survive even at a high temperature up to 1100 K. At low temperature, hundreds of SPEs with a narrow full width at half maxima (FWHM) down to $75 \mu\text{eV}$ are observed which cover a

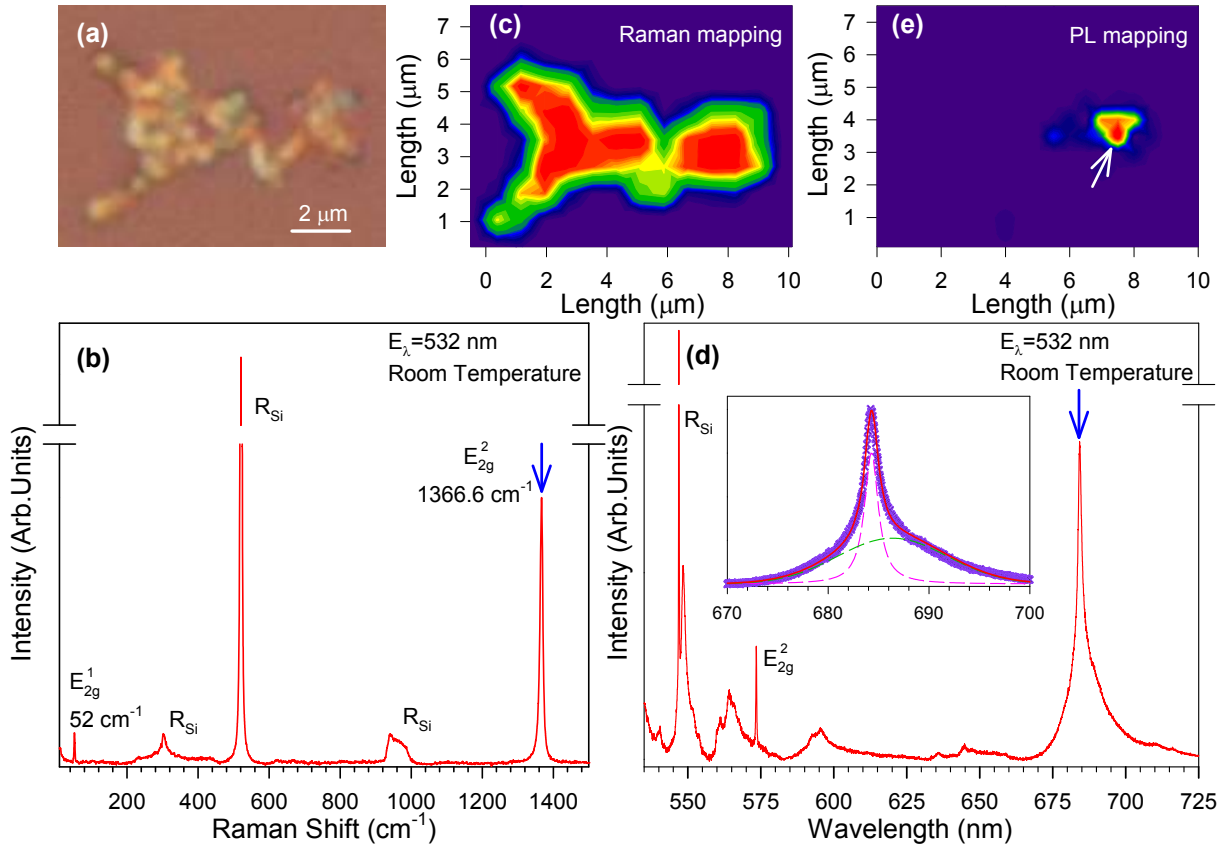


Figure 1 | Raman spectra and defect emission of hBN flakes at room temperature. (a) The optical microscopy image of hBN sample. (b) Raman spectra of hBN samples in (a). (c) Confocal Raman mapping of E_{2g}^2 mode over the same area in (a). (d) PL spectra of defects SPEs of hBN samples in (a), the inset is the fitting results of the defect emission peaks. (e) Confocal PL mapping of defect SPEs over the area in (a) (red color region).

broad spectral band. Such a dense and broadband SPE means that the hBN can be engineered as ultra-broad spectrum SPSs. By using the optical filter or grating, people can easily select arbitrary wavelength SPE in only one hBN chip. Furthermore, we calculate all possible defect levels in hBN based density functional theory, and we found the calculated varieties of defect levels are consistent with our experimental results. Our results can give a better understanding of the defect SPE in hBN and broaden its potential application in quantum technology.

A. Results and Discussions

The samples are commercial hBN flakes suspended in a 50/50 ethanol/water solution (Graphene Supermarket). We dropped cast 30 μL onto a 90 nm SiO_2/Si substrate and waiting for the solvent to dry. We firstly measured the Raman and photoluminescence (PL) spectra of the hBN flakes as shown in Figure 1. Figure 1(a) shows the optical microscopy image of hBN flakes. A typical Raman spectrum of hBN samples at room temperature is depicted in Figure 1(b). Two Raman modes of E_{2g}^1 at

52 cm^{-1} (FWHM= 2.93 cm^{-1}) and E_{2g}^2 at 1366.6 cm^{-1} (FWHM= 10.4 cm^{-1}) are observed, which are consistent with the Raman spectra of exfoliated multilayer hBN in previous reports^{20,40}. Based on the frequency and narrow linewidth of E_{2g}^1 and E_{2g}^2 here, we can confirm that the hBN flakes are multilayer single crystalline. Figure 1(c) shows the corresponding confocal Raman mapping spectra of the E_{2g}^2 mode of hBN at room temperature. Obviously, the shape of the Raman mapping matches with the microscopy image of the hBN sample in Figure 1(a) quite well, which indicates that the samples have uniform crystal quality. Figure 1(d) shows the PL spectra from a certain spot in Figure 1(a) at room temperature. Besides the Raman modes of the silicon substrate and hBN, we observed two bright new peaks around 550 nm and 685 nm from the localized defect states, which have been reported as SPEs in previous studies^{20,24,33,35}. These SPEs in hBN are known to possess a series of zero-phonon lines (ZPL). For defect emission in solid states, the lineshape of ZPL can be governed by the spectra diffusion or phonon broadening mechanisms, which correspond to Gaussian and Lorentzian line shapes⁴¹⁻⁴³, respectively. In general, at low temperature, the lineshape is domi-

nated by the spectral diffusion due to most phonons are in the ground state, whereas at a higher temperature, the phonon broadening mechanism is the dominant factor. Therefore, the lineshape will show a transition from a predominantly Gaussian line shape to a Lorentzian-like shape as the temperature increases from low temperature to room temperature, similar results have also been observed in nanodiamond^{34,41,43}. As a consequence, at room temperature the peak at around 685 nm can be fitted by two components, the narrow one with a Lorentzian shape (~ 4.4 meV) is the ZPL and another broader feature (~ 39 meV) with a Gaussian shape is the phonon sideband⁴⁴. Obviously, the fitting lines match well with the experimental results, as shown in Figure 1(d). Here, the strong ZPL dominates the whole spectra, implying the electron-phonon coupling is weak for SPEs in hBN at room temperature⁴⁴. We also measured the PL mapping of the emission peak at 685 nm as shown in Figure 1(e). In contrast to Raman mapping of the E_{2g}^2 mode, this PL emission only appears at a specific spatial spot, which indicates it comes from the isolated local defect in hBN samples. Similar SPEs in hBN have also been reported by many research groups^{20,22-28,30-35}.

In order to characterize the purity of these SPE, a Hanbury-Brown-Twiss (HBT) setup⁴⁵ is used to measure the second-order correlation function $g^{(2)}(\tau)$. Figure 2(a) shows the representative PL spectrum of one isolated hBN defect, and Figure 3(b-c) shows the measured $g^{(2)}(\tau)$ and fitting results. Here $g^{(2)}(\tau) = 1 - ae^{-|\tau|/\tau_0}$, where a is the background of uncorrelated photons and τ_0 is the antibunching recovery time. By fitting the experimental data, the value of $g^{(2)}(0)$ for the SPEs at around 595 (P1) and 685 nm (P2) are equal to 0.09 and 0.06, respectively. Both of these two values are below than 0.1, which unambiguously proving that the defect emitters here are high purity SPEs. The lifetimes of these SPEs were also measured by time-resolved PL spectroscopy, as shown in Figure 3(d-e). Based on the fitting results, the lifetime of P1 and P2 are ~ 1.12 and 1.35 ns, respectively, consistent with lifetime values 1.0 ns and 1.4 ns deduced from the fitted line-width of $g^{(2)}(\tau)$ functions, respectively.

To fully understand the relationship between defect SPEs and excitation wavelength, we have further conducted the PLE mapping of the defect emission at room temperature, as shown in Figure 3(a). Remarkably, we found that the intensity and wavelength of these SPEs are strongly dependent on the excitation wavelength. The dashed lines correspond to the defect levels involved in the excitation-emission process. The emission at around 685 nm, 750 nm, and 767 nm are greatly enhanced when the excitation wavelengths are around at 490 nm, 494 nm, and 528 nm, respectively. These two peaks at 685 nm and 750 nm are also enhanced at around 478 nm and 546 nm, but their intensities are weaker than the formers. In particular, the emission at around 711 nm is only greatly enhanced under excitation at around 500 nm and slightly enhanced at around 472 nm. While for other

excitation wavelengths, these defect SPEs are too weak to be observed. To make it clearer, partially extracted spectra are presented in Figure S1(a). Clearly, different emissions have different resonance excitation profiles as well as a different emission wavelength, as shown in Figure S1(b). The excitation selectivity of the PLE spectra typically contains a distinct resonance behavior, suggesting that many real intermediate defect energy levels are involved in these defect emission processes. Furthermore, both of the emissions at 685 nm and 750 nm are enhanced under 494 nm and 528 nm excitation wavelength. The energy difference between these two resonant excitation peaks (494 nm and 528 nm) is around 162 meV, which is very close to the energy of E_{2g}^2 phonon mode (around 169 meV), implying the phonon plays an important role in defect SPEs of hBN. Such a strictly resonant condition between one phonon and two atomic-like individual defect level states provides a good platform to achieve phonon ground cooling and amplification by using a resolved sideband Raman cooling technique as reported in semiconductor ZnTe^{46,47}, as well as quantum coherent state manipulation based on phonon-single photon coupling².

Considering the selectivity resonance-enhanced SPEs in hBN, we have tried to measure many sample positions with different excitation wavelengths ranging from ultraviolet to near-infrared. Figure 3(b) shows the corresponding results measured by six laser lines. Interestingly, we observed a series of narrow SPEs from 357 nm to 896 nm at room temperature, much broader than previously reported results that mainly spans from 550 nm to 800 nm^{24,38,39}. These emissions are also localized in a specific sample point. We should note that the intensities of these emitters below 400 nm and over 800 nm are weaker compared to the emitters at other spectral ranges, which may be caused by the harsh requirement to achieve resonance excitation. And among these excitation wavelengths, the 442 nm excitation can obtain more dense and bright SPEs. The different behaviors of emitters in hBN also mean that the electronic level and crystallographic structure of the emitters are much more complexes than current theoretical proposals^{20,48,49}. The emission intensity of defect SPE in hBN is heavily dependent on the excitation photon wavelength also explains why we can observe the defect emissions from ultraviolet to near-infrared by using different excitation wavelengths. In short, different emitters have different emission wavelengths and these emissions also have different resonance behaviors as well. Therefore, if the excitation wavelengths match isolated defect energy levels well, the SPEs in hBN with brighter intensity and wider spectral range are supposed to be observed.

Since the photostability of SPEs over time is very important for SPS application in quantum technology, we measured the temporal evolution of defect emitters at around 477, 685 and 796 nm, as shown in figure 3(c). It is obvious that the frequency and intensity of these emissions almost remain unchanged with time, suggesting

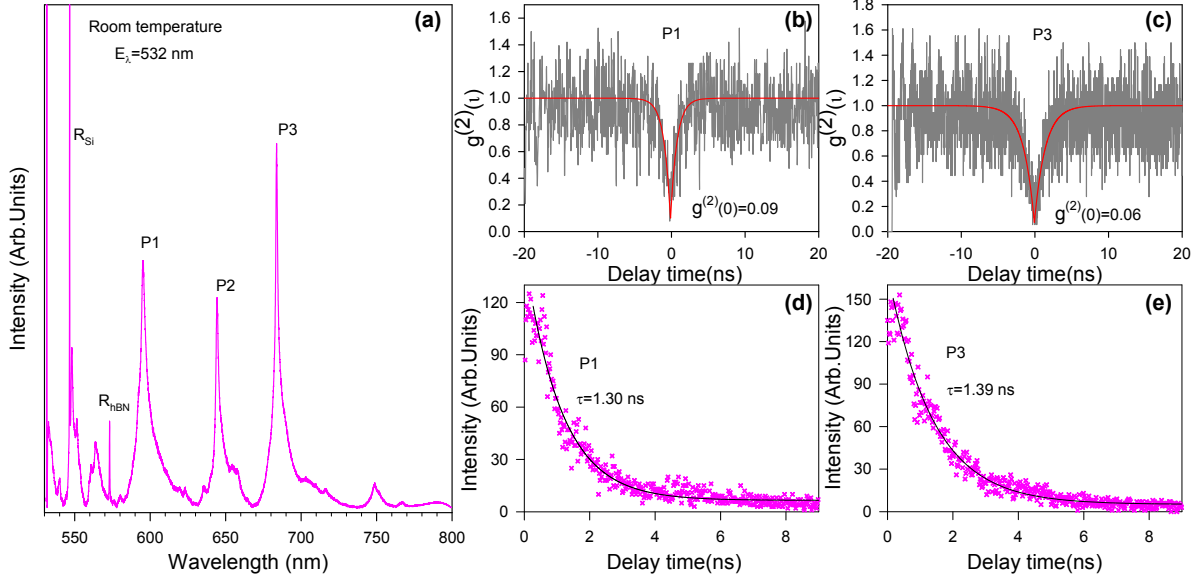


Figure 2 | Observation of photon antibunching at room temperature. (a) The PL spectra of localized emitter. (b-c) The second-order correlation measurement of peak 1 (P1) and peaks 3 (P3) in (a), respectively. The red line is the fitting results to the experimental data. (d-e) Time-resolved PL of peak 1 (P1) and peaks 3 (P3) in (a), respectively. The black line is the fitting results to the experimental data.

these emitters are very stable. These results are similar to previous reports about the color center in diamond⁵⁰. In contrast to these stable SPEs, we also found that only a few defect emitters show a slighter fluorescence blinking behavior as shown in Figure S2, similar results have also been observed by other groups.^{22,32,37} Here we find the blinking emitters are only dependent on the sample location but not on the excitation wavelength. It means that the local environment of defects is the dominant mechanism for the SPE blinking in hBN flakes. Furthermore, we also measured the intensity saturation behaviors of the defect SPEs at 477 nm, 577 nm, 685 nm, and 796 nm as a function of the excitation power, as shown in Figure 3(d). The data can be fitted by a simple saturation function: $I = I_{\infty} P / (P + P_{sat})$, where I_{∞} and P_{sat} are the emission rate and excitation power at saturation, respectively. We find the saturation emission rate I_{∞} are equal to 1.7×10^4 , 0.3×10^4 , 1.2×10^4 and 0.7×10^4 counts/s for the emissions at 477 nm, 577 nm, 685 nm and 796 nm, respectively, and P_{sat} are equal to 5.61×10^4 , 2.9×10^4 , 3.96×10^4 and 3.03×10^4 W/cm² for the emissions at 477 nm, 577 nm, 685 nm and 796 nm, respectively. These results are consistent with previously reported results that the SPE in hBN is the brightest SPE reported so far among the 2D materials SPE library². On the other hand, the saturation behavior also indicates that the defect emissions are photostable even under high laser excitation power.

Because of the low temperature environment would greatly suppress the non-radiative process and phonon broadening of SPEs, the SPEs in hBN with much nar-

rower linewidth and much brighter intensity are expected to be observed. In order to observe SPEs as much as possible from hBN flakes, we used the 442 nm (2.81 eV) laser as the excitation wavelength to measure the SPEs at low temperature, as shown in Figure 4(a) and Figure S3. Surprisingly, in contrast to only several single photon peaks appeared at one selected isolated defect at room temperature, there are hundreds of peaks appeared at one isolated defect location as the temperature drops to around 4 K. The SPE at low temperature here cover a wide spectral range from 2.80 eV (443 nm) to 1.544 eV (803 nm), and each different isolated position also has a different emission spectrum, as shown in Figure 4(a). It implies that the hBN based SPEs can achieve a broadband SPSs covering from near-ultraviolet to near-infrared spectral range. In particular, these SPE peaks show an ultra-narrow linewidth down to ~ 75 μ eV, as shown in Figure 4(a) inset and Figure S3. We note that this value is very close to the narrowest linewidth of ~ 45 μ eV reported in the prepared hBN samples on Al_2O_3 substrate³². However, the intrinsic linewidth of SPE here may be less than ~ 75 μ eV if the resolution of our spectrometer is counted. We also measured the photostability of SPEs overtime at 4 K, as shown in Figure S4. Obviously, most SPEs are very stable and few of them show a blinking behavior over time.

To further confirm purity of these SPEs at low temperature, we also measured $g^{(2)}(\tau)$ functions of two typical defect emissions at around 587 and 694 nm, respectively, as shown in Figure S5. Both of $g^{(2)}(0)$ values are 0.08 and 0.02, suggesting there are high purity SPEs. We also

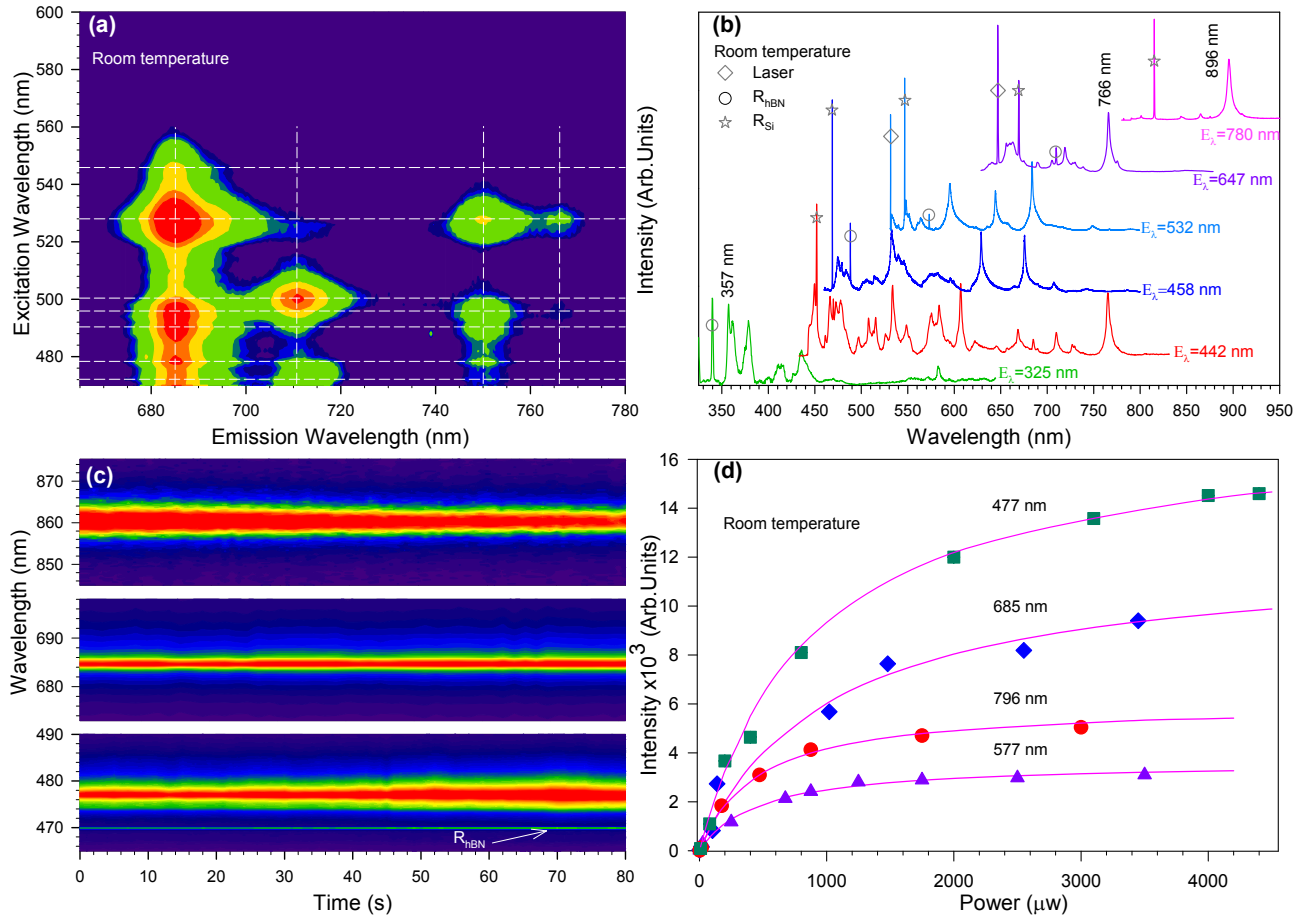


Figure 3 | Observation of a broad spectral range of defect SPEs in hBN at room temperature. (a) The confocal PLE mapping of one selectively isolated defect emission at room temperature, the white dash lines are used to guide the resonance enhancement excitation wavelength and emission wavelength. (b) PL spectra of different position in hBN with six different excitation wavelengths at room temperature. The star, circle and diamond symbols mark the Raman mode of silicon, E_{2g}^2 mode of hBN and the laser line, respectively. (c) The temporal evolution of three different defect emitters under continuous illumination at room temperature. (d). The intensity of emitters centered at 477, 577, 685 and 796 nm from the different position as a function of laser power at room temperature, respectively.

measured the SPEs from isolated defect in hBN by using 532 nm (2.34 eV) excitation wavelength (energy), as shown in Figure S6. Similar to the results that measured by 442 nm, multiple defect emission peaks appeared at one selected point. However, the number of observed single photon peaks is considerably reduced. This is another evidence of selectively resonance enhanced SPEs as discussed above.

Now we try to analyze the underlying physical mechanisms that caused such a dense broad spectrum SPEs appeared at low temperature. Although there is a slight difference among the emission spectrum at each different location, they still share some similar characters. According to the density of SPEs, we simply divided the measured spectra into seven bands, and mark them with different background colors, as shown in Figure 4(a-b). We suspect that these different regions may correspond

to different defect types in hBN^{20,37,48}. Because the hBN flakes sample is prepared in organic solution, there are likely to produce many defects, such as H and O atom substitutional, or boron vacancy and carbon interstitial. We also calculated the energy level of different defect types and will discuss below. Another possible speculation is there are many phonon replicas of SPE, leading to the observation of such dense emissions^{51,52}. In addition, there are many fine intermediate defect levels already located in the band gap of hBN. However, owing to the two-dimensional nature of the host material, these defect emitters are highly exposed to its localized surroundings environments^{30,34,36,37}. Considering their different types of defects and local environments⁴⁸, only a few of them are optically active or stable under ambient conditions. When the sample is at a low-temperature environment, more fine structures of defect states become

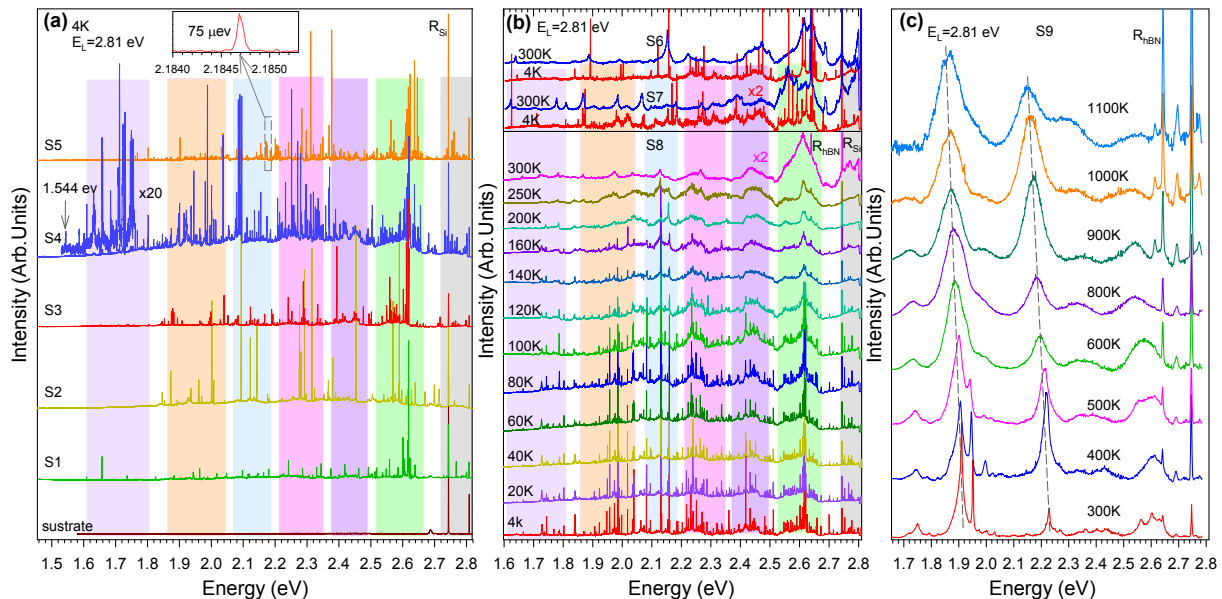


Figure 4 | Observation of single photon emission in hBN from 4 K to 1100 K. (a) PL spectra of different position in hBN with excitation wavelength 442 nm (2.81 eV) at 4 K. The inset one is the extracted PL with a narrow range from position 5. (b) The upper part is defect SPEs from two different spots at 4 K and room temperature, respectively. The bottom part is the evolution of defect SPEs from another position with temperature from 4 K to 300 K. (c) PL spectra of defect emissions with excitation wavelength 442 nm from 300 K to 1100 K.

activated and the transition between them is allowed. So that we can observe abundant SPEs under this condition. Besides, the quantum efficiency of SPEs is enhanced and the linewidth broadening of fine structures of defect states is strongly suppressed at low temperature⁴¹, thus more SPEs become resolvable. In order to further confirm the above speculations, we performed temperature-dependent measurements of SPEs in hBN from 4 K to room temperature, as shown in Figure 4(b). Obviously, each band of SPEs at low temperature evolves into one broad defect emission peak above 140 K, and the intensities are greatly reduced. The temperature dependent experiments are consistent with our previous analysis, indicating our speculations are relatively reasonable.

Room temperature or even higher temperature operation is desired for the real application of SPS. We measured one SPEs from room temperature to 1100 K, as shown in Figure 4(c). Remarkably, these SPE peaks can still survive even when the temperature is increased up to 1100 K. As the temperature increase, the linewidth of these SPE peaks are widened, and the emission wavelengths are redshift, which is consistent with the previous reports²⁹. Although the whole intensities of these emissions decreases as temperature increases, the relative intensities are different. For example, the emission at around 2.23 eV (556 nm) is weak at room temperature, but the intensity is enhanced at around 400 K, and then slowly decreases with temperature increases. The purity of these emissions at high temperatures and detailed physical mechanism behind this phenomenon calls for further studies.

To give a better understanding of the origin of such broadband emission, we calculated the electronic energy band structures of the monolayer and bulk hBN, as well as its possible defect states related with H, O, C, N and B induced defects based on the density functional theory (DFT), as shown in Fig. 5(a). The calculated band gaps of hBN are 5.94 and 5.98 eV for the monolayer and bulk hBN, respectively, which are consistent with previous experimental results⁵³. More calculation details were shown in Supplementary Information. We used the short straight lines to denote the defect states in Fig. 5(a). The blue lines indicate the defect states are fully filled with electrons, which possess the possibility for electrons transit into the conduction band. The red lines denote the empty defect states, which indicate that here the holes maybe transfer to the valence band. The black straight lines represent the defect states which are half filled with electrons. Therefore, it is possible for electrons transition to the conduction band and the holes transition down to the valence band. Fig. 5(c) shows all possible transition energies of various native defects and impurities states. Every column represents the different types of defect states. The blue and red columns represent defect states in monolayer hBN, and white and pink columns represent defect states in bulk hBN, for instance, the emission energies at around 1.5 eV may correspond to C_B , C_N and V_B defect type, and 2.3 eV and 3 eV may correspond to the H_N and V_B defect type, respectively. Therefore, the defect types in Fig 2 may correspond to H_N and V_N . In addition, the defect types in monolayer and bulk hBN are almost the same, but the

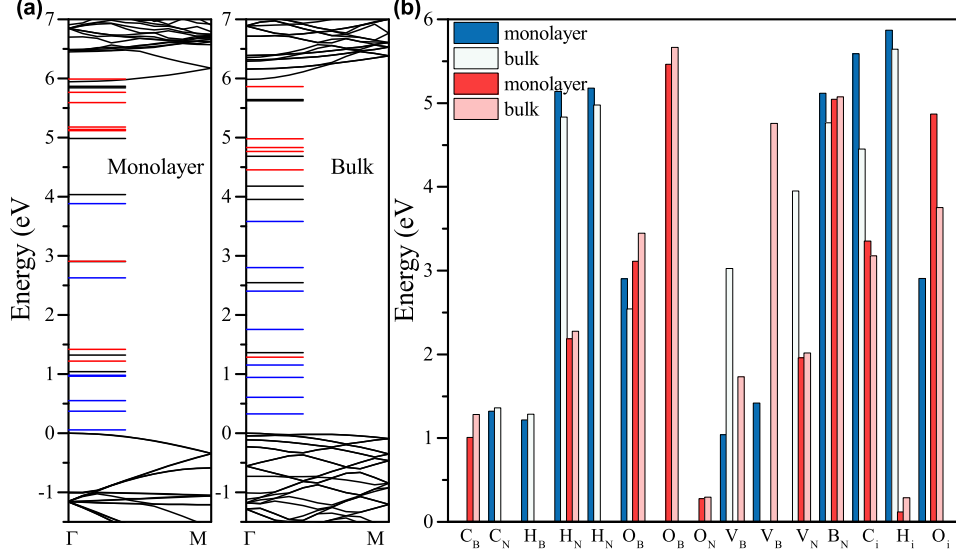


Figure 5 | Calculation of defect levels in monolayer and bulk hBN. (a) Band structure of the monolayer h-BN and bulk h-BN with defect states. The blue lines indicate the defect states are fully filled with electrons, the black straight lines represent the defect states which are half filled with electrons, and the red lines denote the empty defect states. The energy of the host valence band maxima is set to zero. (c) The neutral state transition energies for various native defects and impurities. The blue and red columns represent defects in monolayer hBN, and white and pink columns represent defects in bulk hBN. C_B denotes a C impurity substituting for a lattice B atom, and boron vacancy and carbon interstitial are denoted by V_B and C_i , respectively.

energies have a slightly difference, indicating the energy is small varied in different thickness hBN for the same defect type. Similarly, the same defect type may own multiple emission levels. Therefore, for different hBN samples, its different thickness will have a small effect on the defect emission wavelength. Remarkably, the calculated defect levels both in monolayer and bulk hBN are ranged from infrared to ultraviolet region, which are consistent with our experimental results. Meanwhile, we found the number of defect types in infrared range is relatively few, making it difficult to find one location with an emission wavelength in the infrared region. However, for some different defect types in bulk (or monolayer) case, they may share the same energy level (e.g., V_B and C_B , O_B and O_i). Therefore, it is hard to directly identify all the defect types just according to the measured PL spectrum and calculated results. In this case, the transmission electron microscope and ion implantation may be good methods to help further identify the defect types. To fully understand these defect types, and to controllably prepare the SPEs in hBN, more works are required in the future.

B. Conclusion

In conclusion, we have observed an ultra-broad spectral range SPEs from ultraviolet to near-infrared in hBN. Most of these isolated emitters show a photostability and high brightness under ambient conditions and even when the temperature up to 1100 K. We also found these SPEs in hBN are strongly dependent on the excitation wavelength. At low temperature, up to hundreds of defect emissions with ultra-narrow linewidth are observed. Such dense SPEs at low temperature suggest that the SPE defects in hBN have much more complex level structures. We also calculated the defect level of monolayer and bulk hBN based on DFT method. And we found the energies of defect levels are ranged from infrared to ultraviolet region, which are consistent with our experimental results. Our results not only provide a better understanding of the level structure of the defect emitters in hBN, but also show that the hBN is a good host material for constructing an ultraviolet to near-infrared broad-spectrum single photon source. These novel properties of hBN hold a great promise for its application in quantum technology.

C. Experimental Section

Sample Preparation The hBN flakes are suspended in a 50/50 water/ethanol solution (Graphene Supermarket). A 20 μL solution is dispersed onto a 90 nm SiO_2/Si substrate.

Optical Measurement Confocal Raman and PL measurements on hBN samples were undertaken in backscattering geometry with a Jobin-Yvon HR800 system equipped with a liquid-nitrogen-cooled charge-coupled detector. The Raman and PL measurements at room temperature were undertaken with a 100X objective lens (NA=0.9) (or a 39X UV objective) and 100 and 600 lines mm^{-1} grating at room temperature. The Montana cryostat system was employed to cool the samples down to 4 K under a vacuum of 0.2 mTorr. A 50X long-working-distance objective lens (NA=0.5) and both 600 and 2400 lines mm^{-1} grating were used for PL measurements at low temperature. The excitation laser (E_L) line 458 nm is from an Ar^+ laser, 647 nm is from a He-Ne laser, 532 nm and 780 nm are from an Nd: YAG laser, 325 nm and 442 nm are from an He-Cd laser. The confocal PLE measurements are carried out by using house-built confocal microscopic PLE system, where a super continuous laser source combined with a grating monochromator is used as excitation source. The second-order correlation function measurement is carried out by using home-built Hanbury-Brown-Twiss (HBT) setup.

Acknowledgement

We acknowledge support from National Basic Research Program of China (grant no. 2016YFA0301200, 2017YFA0303401), NSFC (11574305, 51527901, 11474277, 11434010 and 11225421) and LU JIAXI International team program supported by the K.C. Wong Education Foundation and the Chinese Academy of Sciences. J. Z. also acknowledges support from National Young 1000 Talent Plan of China.

Author Contribution

J.Z. and Q.T conceived the ideas; Q.T., B.S., P.T. and J.Z. designed the experiments. Q.T., X.L., S.R. and Y.G prepared the samples. Q.T., X.L., Y.X., and X.D. performed experiments. D.G. and H.D performed the calculations. Q.T. and Z.J. analyzed the data and wrote the manuscript with inputs from all authors.

Competing interests:

The authors declare that they have no competing financial interests.

Additional information

Supplementary information is available in the online version of the paper. Reprints and permissions information is available online.

Correspondence and requests for materials should be addressed to J.Z. (Email: zhangjwill@semi.ac.cn).

-
- ¹ B. Lounis and M. Orrit, Rep. Prog. Phys. **68**, 1129 (2005)
- ² I. Aharonovich, D. Englund, and M. Toth, Nat. Photonics **10**, 631 (2016)
- ³ W. B. Gao, A. Imamoglu, H. Bernien, and R. Hanson, Nat. Photonics **9**, 363 (2015)
- ⁴ P. Lodahl, S. Mahmoodian, and S. Stobbe, Rev. Mod. Phys. **87**, 347 (May 2015)
- ⁵ P. Kok, W. J. Munro, K. Nemoto, T. C. Ralph, J. P. Dowling, and G. J. Milburn, Rev. Mod. Phys. **79**, 135 (Jan 2007)
- ⁶ C. Santori, D. Fattal, J. Vuckovic, G. S. Solomon, and Y. Yamamoto, New J. Phys. **6**, 89 (2004)
- ⁷ P. Senellart, G. Solomon, and A. White, Nat. Nanotechnol. **12**, 1026 (2017)
- ⁸ X. Ma, N. F. Hartmann, J. K. Baldwin, S. K. Doorn, and H. Htoon, Nat. Nanotechnol. **10**, 671 (2015)
- ⁹ C. Chakraborty, L. Kinnischtzke, K. M. Goodfellow, R. Beams, and A. N. Vamivakas, Nat. Nanotechnol. **11**, 7 (2015)
- ¹⁰ A. Srivastava, M. Sidler, A. V. Allain, D. S. Lembke, A. Kis, and A. Imamoglu, Nat. Nanotechnol. **10**, 491 (2015)
- ¹¹ M. Koperski, K. Nogajewski, A. Arora, V. Cherkez, P. Mallet, J. Y. Veuillen, J. Marcus, P. Kossacki, and M. Potemski, Nat. Nanotechnol. **10**, 503 (2015)
- ¹² Y. M. He, ClarkGenevieve, R. SchaibleyJohn, Y. He, ChenMing, C. WeiYu, J. DingXing, Q. Zhang, W. Yao, X. Xu, C.-Y. Lu, and J.-W. Pan, Nat. Nanotechnol. **10**, 497 (2015)
- ¹³ C. Chakraborty, L. Kinnischtzke, K. M. Goodfellow, R. Beams, and A. N. Vamivakas, Nat. Nanotechnol. **10**, 507 (2015)
- ¹⁴ P.-B. Carmen, D. M. Kara, A. R. P. Montblanch, M. Barbone, P. Latawiec, D. Yoon, A. K. Ott, M. Loncar, A. C. Ferrari, and M. Atatre, Nat. Commun. **8**, 15093 (2017)
- ¹⁵ P. B. Carmen, B. Matteo, D. M. Kara, X. Chen, G. Ilya, Y. Duhee, A. K. Ott, B. Jan, W. Kenji, and T. Takashi, Nat. Commun. **7**, 12978 (2016)
- ¹⁶ M. J. Holmes, K. Choi, S. Kako, M. Arita, and Y. Arakawa, Nano Lett. **14**, 982 (2014)
- ¹⁷ A. M. Berhane, K. Jeong, Z. Bodrog, S. Fiedler, T. Schröder, N. V. Trivoo, T. Palacios, A. Gali, M. Toth, and D. Englund, Adv. Mater. **29**, 1605092 (2017)
- ¹⁸ Y. Zhou, Z. Wang, A. Rasmita, S. Kim, A. Berhane, Z. Bodrog, G. Adamo, A. Gali, I. Aharonovich, and W.-b. Gao, Science Advances **4**, eaar3580 (2018)
- ¹⁹ S. Kako, C. Santori, K. Hoshino, S. GoTzinger, Y. Yamamoto, and Y. Arakawa, Nat. Mater. **5**, 887 (2006)
- ²⁰ T. T. Tran, K. Bray, M. J. Ford, M. Toth, and I. Aharonovich, Nat. Nanotechnol. **11**, 37 (2015)
- ²¹ T. T. Tran, C. Zachreson, A. M. Berhane, K. Bray, R. G. Sandstrom, L. H. Li, T. Taniguchi, K. Watanabe, I. Aharonovich, and M. Toth, Phys. Rev. Appl. **5**, 034005 (Mar 2016)
- ²² L. J. Martínez, T. Pelini, V. Waselowski, J. R. Maze, B. Gil, G. Cassabois, and V. Jacques, Phys. Rev. B **94**, 121405 (Sep 2016)

- ²³ N. R. Jungwirth, B. Calderon, Y. Ji, M. G. Spencer, M. E. Flatt, and G. D. Fuchs, *Nano Lett.* **16**, 6052 (2016)
- ²⁴ T. T. Tran, C. Elbadawi, D. Totonjian, C. J. Lobo, G. Grosso, H. Moon, D. R. Englund, M. J. Ford, I. Aharonovich, and M. Toth, *ACS Nano* **10**, 7331 (2016)
- ²⁵ Z. Shotan, H. Jayakumar, C. R. Consideine, M. Mackoitt, H. Fedder, J. Wrachtrup, A. Alkauskas, M. W. Doherty, V. M. Menon, and C. A. Meriles, *ACS Photonics* **3**, 2490 (2016)
- ²⁶ R. Bourrellier, S. Meuret, A. Tararan, O. Stphan, M. Kociak, L. H. G. Tizei, and A. Zobelli, *Nano Lett.* **16**, 4317 (2016)
- ²⁷ N. Chejanovsky, M. Rezai, F. Paolucci, Y. Kim, T. Rendler, W. Rouabeh, F. Favaro de Oliveira, P. Herlinger, A. Denisenko, S. Yang, I. Gerhardt, A. Finkler, J. H. Smet, and J. Wrachtrup, *Nano Lett.* **16**, 7037 (2016)
- ²⁸ A. W. Schell, T. T. Tran, H. Takashima, S. Takeuchi, and I. Aharonovich, *APL Photonics* **1**, 091302 (2016)
- ²⁹ M. Kianinia, B. Regan, S. A. Tawfik, T. T. Tran, M. J. Ford, I. Aharonovich, and M. Toth, *ACS Photonics* **4**, 768 (2017)
- ³⁰ A. L. Exarhos, D. A. Hopper, R. R. Grote, A. Alkauskas, and L. C. Bassett, *ACS Nano* **11**, 3328 (2017)
- ³¹ T. T. Tran, D. Wang, Z.-Q. Xu, A. Yang, M. Toth, T. W. Odom, and I. Aharonovich, *Nano Lett.* **17**, 2634 (2017)
- ³² X. Li, G. D. Shepard, A. Cupo, N. Camporeale, K. Shayan, Y. Luo, V. Meunier, and S. Strauf, *ACS Nano* **11**, 6652 (2017)
- ³³ N. R. Jungwirth and G. D. Fuchs, *Phys. Rev. Lett.* **119**, 057401 (Jul 2017)
- ³⁴ B. Sontheimer, M. Braun, N. Nikolay, N. Sadzak, I. Aharonovich, and O. Benson, *Phys. Rev. B* **96**, 121202 (Sep 2017)
- ³⁵ G. Grosso, H. Moon, B. Lienhard, S. Ali, D. K. Efetov, M. M. Furchi, P. Jarillo-Herrero, M. J. Ford, I. Aharonovich, and D. Englund, *Nat. Commun.* **8**, 705 (2017)
- ³⁶ A. W. Schell, M. Svedendahl, and R. Quidant, *Adv. Mater.* **30**, 1704237 (2018), <https://onlinelibrary.wiley.com/doi/abs/10.1002/adma.201704237>
- ³⁷ M. Koperski, K. Nogajewski, and M. Potemski, *Optics Communications* **411**, 158 (2018), ISSN 0030-4018
- ³⁸ A. Dietrich, M. Bürk, E. S. Steiger, L. Antoniuk, T. T. Tran, M. Nguyen, I. Aharonovich, F. Jelezko, and A. Kubanek, *Phys. Rev. B* **98**, 081414 (2018), <https://link.aps.org/doi/10.1103/PhysRevB.98.081414>
- ³⁹ Z.-Q. Xu, C. Elbadawi, T. T. Tran, M. Kianinia, X. Li, D. Liu, T. B. Hoffman, M. Nguyen, S. Kim, J. H. Edgar, X. Wu, L. Song, S. Ali, M. Ford, M. Toth, and I. Aharonovich, *Nanoscale* **10**, 7957 (2018), <http://dx.doi.org/10.1039/C7NR08222C>
- ⁴⁰ R. V. Gorbachev, I. Riaz, R. R. Nair, R. Jalil, L. Britnell, B. D. Belle, E. W. Hill, K. S. Novoselov, K. Watanabe, T. Taniguchi, A. K. Geim, and P. Blake, *Small* **7**, 465 (2011)
- ⁴¹ T. Müller, I. Aharonovich, Z. Wang, X. Yuan, S. Castelletto, S. Praver, and M. Atatüre, *Phys. Rev. B* **86**, 195210 (Nov 2012)
- ⁴² J. Wolters, N. Sadzak, A. W. Schell, T. Schröder, and O. Benson, *Phys. Rev. Lett.* **110**, 027401 (Jan 2013)
- ⁴³ E. Neu, C. Hepp, M. Hauschild, S. Gsell, M. Fischer, H. Sternschulte, D. Steinmüller-Nethl, M. Schreck, and C. Becher, *New Journal of Physics* **15**, 043005 (2013)
- ⁴⁴ J. Friedrich and D. Haarer, *Angew. Chem. Int. Ed.* **23**, 113 (1984), ISSN 1521-3773
- ⁴⁵ R. Hanbury-Brown and R. Q. Twiss, *Nature* **177**, 27 (1956)
- ⁴⁶ J. Zhang, Q. Zhang, X. Wang, L. C. Kwek, and Q. Xiong, *Nat Photon* **10**, 600 (2016)
- ⁴⁷ J. Zhang, D. Li, R. Chen, and Q. Xiong, *Nature* **493**, 504 (2013)
- ⁴⁸ S. A. Tawfik, S. Ali, M. Fronzi, M. Kianinia, T. T. Tran, C. Stampfl, I. Aharonovich, M. Toth, and M. J. Ford, *Nanoscale* **9**, 13575 (2017)
- ⁴⁹ M. Abdi, M.-J. Hwang, M. Aghtar, and M. B. Plenio, *Phys. Rev. Lett.* **119**, 233602 (Dec 2017)
- ⁵⁰ K. Li, Y. Zhou, A. Rasmita, I. Aharonovich, and W. B. Gao, *Phys. Rev. Appl.* **6**, 024010 (Aug 2016)
- ⁵¹ X. Chen, X. Lu, S. Dubey, Q. Yao, S. Liu, X. Wang, Q. Xiong, L. Zhang, and A. Srivastava, *Nat. Phys.* **15**, 221 (2019)
- ⁵² M. A. Feldman, A. Poretzky, L. Lindsay, E. Tucker, D. P. Briggs, P. G. Evans, R. F. Haglund, and B. J. Lawrie, *Phys. Rev. B* **99**, 020101 (2019)
- ⁵³ G. Cassabo, P. Valvin, and B. Gil, *Nature Photonics* **10**, 262 (2016)